NASA/TM-20240013567 AIAA 2025–1640

Piloted Evaluation of a Fault Recovery System for an Aircraft with Distributed Electric Propulsion

Jonathan S. Litt and Jonah J. Sachs-Wetstone
Glenn Research Center, Cleveland, Ohio

T. Shane Sowers
HX5, LLC, Brook Park, Ohio 44142

A. Karl Owen
NovaTek Engineering, Chardon, Ohio 44024

Sophia M. Bricker and Anna Schaldenbrand
Glenn Research Center, Cleveland, Ohio

January 2025

NASA STI Program Report Series

Since its founding, NASA has been dedicated to the advancement of aeronautics and space science. The NASA scientific and technical information (STI) program plays a key part in helping NASA maintain this important role.

The NASA STI program operates under the auspices of the Agency Chief Information Officer. It collects, organizes, provides for archiving, and disseminates NASA's STI. The NASA STI program provides access to the NTRS Registered and its public interface, the NASA Technical Reports Server, thus providing one of the largest collections of aeronautical and space science STI in the world. Results are published in both non-NASA channels and by NASA in the NASA STI Report Series, which includes the following report types:

- TECHNICAL PUBLICATION.
  Reports of completed research or a major significant phase of research that present the results of NASA programs and include extensive data or theoretical analysis. Includes compilations of significant scientific and technical data and information deemed to be of continuing reference value. NASA counterpart of peer-reviewed formal professional papers but has less stringent limitations on manuscript length and extent of graphic presentations.

- TECHNICAL MEMORANDUM.
  Scientific and technical findings that are preliminary or of specialized interest, e.g., quick release reports, working papers, and bibliographies that contain minimal annotation. Does not contain extensive analysis.

- CONTRACTOR REPORT.
  Scientific and technical findings by NASA-sponsored contractors and grantees.

- CONFERENCE PUBLICATION.
  Collected papers from scientific and technical conferences, symposia, seminars, or other meetings sponsored or cosponsored by NASA.

- SPECIAL PUBLICATION.
  Scientific, technical, or historical information from NASA programs, projects, and missions, often concerned with subjects having substantial public interest.

- TECHNICAL TRANSLATION.
  English-language translations of foreign scientific and technical material pertinent to NASA's mission.

Specialized services also include organizing and publishing research results, distributing specialized research announcements and feeds, providing information desk and personal search support, and enabling data exchange services.

For more information about the NASA STI program, see the following:

- Access the NASA STI program home page at http://www.sti.nasa.gov

NASA/TM-20240013567 AIAA 2025–1640

Piloted Evaluation of a Fault Recovery System for an Aircraft with Distributed Electric Propulsion

Jonathan S. Litt and Jonah J. Sachs-Wetstone
Glenn Research Center, Cleveland, Ohio

T. Shane Sowers
HX5, LLC, Brook Park, Ohio 44142

A. Karl Owen
NovaTek Engineering, Chardon, Ohio 44024

Sophia M. Bricker and Anna Schaldenbrand
Glenn Research Center, Cleveland, Ohio

Prepared for the
SciTech Forum
sponsored by the American Institute of Aeronautics and Astronautics
Orlando, Florida, January 6–10, 2025

National Aeronautics and
Space Administration

Glenn Research Center
Cleveland, Ohio 44135

January 2025

Acknowledgments

The Transformative Aeronautics Concepts Program (TACP)/Convergent Aeronautics Solutions Project sponsors this work with the support of the Transformational Tools and Technologies Project, also under the TACP, which is under the NASA Aeronautics Research Mission Directorate.

This work was sponsored by the
Transformative Aeronautics Concepts Program.

Level of Review: This material has been technically reviewed by technical management.

This report is available in electronic form at https://www.sti.nasa.gov/ and https://ntrs.nasa.gov/

NASA STI Program/Mail Stop 050
NASA Langley Research Center
Hampton, VA 23681-2199

Piloted Evaluation of a Fault Recovery System for an Aircraft with Distributed Electric Propulsion

Jonathan S. Litt and Jonah J. Sachs-Wetstone
National Aeronautics and Space Administration
Glenn Research Center
Cleveland, Ohio 44135

T. Shane Sowers
HX5, LLC
Brook Park, Ohio 44142

A. Karl Owen
NovaTek Engineering
Chardon, Ohio 44024

Sophia M. Bricker* and Anna Schaldenbrand†
National Aeronautics and Space Administration
Glenn Research Center
Cleveland, Ohio 44135

Abstract

Electrified aircraft powertrains contain multiple tightly coupled subsystems, making them much more complex than traditional aircraft propulsion systems, both in terms of integration and control. Electrification enables aircraft to have multiple distributed thrust-producing fans that the flight control system can utilize for enhanced maneuverability, further increasing the control complexity. The SUbsonic Single Aft eNgine (SUSAN) Electrofan is a NASA concept aircraft that leverages this technology. SUSAN is a series/parallel partial hybrid electric single-aisle transport aircraft that takes advantage of its electrified powertrain to provide fuel burn and emissions benefits when compared to the state-of-the-art. Achieving these benefits requires an appropriately designed control architecture that coordinates the various powertrain and flight control subsystems. As such, the SUSAN aircraft is designed with a high level of automation, allowing it to properly manage coupled subsystems and react rapidly to failures and anomalies. To do this effectively, algorithms that perform component health management, fault detection, isolation, and accommodation, and continuous optimization, must be developed, tested, validated, and implemented. This paper describes a piloted evaluation of such an algorithm in scenarios with multiple fan failures, performed in a flight simulator, demonstrating failure recovery and continued safe operation up to the limits of the powertrain. These scenarios are subsequently related to certification requirements.

1.0 Introduction

The SUbsonic Single Aft eNgine (SUSAN) Electrofan (Figure 1) is a subsonic regional jet transport aircraft concept that utilizes electrified aircraft propulsion (EAP) technologies to enable propulsive and

* NASA Office of STEM Engagement Summer 2024 Intern, Institut National des Sciences Appliquées (INSA) of Lyon undergraduate.
† NASA Office of STEM Engagement Summer 2024 Intern, Cornell University undergraduate.

aerodynamic benefits to reduce fuel usage, emissions, and cost. The target market is the regional low-cost carrier airline with mission specification: 180 passengers, design range of 2,500 miles, economic range of 750 miles, and speed of Mach 0.78 (Ref. 1). The details of the concept are evolving as the design matures (Refs. 1 and 2), but consistent features include a single aft-mounted boundary layer-ingesting (BLI) turbofan gas turbine engine (GTE) with generators driving a series/parallel partial hybrid EAP system (Figure 2). The current iteration of SUSAN has 16 underwing two-stage contrarotating fans (Electric Engines or EEs), eight on each side. Note that for this paper, Electric Engine is used to mean the entire contrarotating fan, including the electric motor, controller, etc., used as the source of propulsion. Generally, a single GTE would present a certification problem as an engine failure could prove catastrophic. The SUSAN concept attempts to overcome this with single-use (primary) batteries that provide emergency power to the EEs in case of GTE or generator failure. Relatively small reusable (secondary) batteries are also present to enable various EAP benefits. A diagram of the powertrain is shown in Figure 3 (Ref. 2). To fully realize the benefits of the SUSAN design, the operation of the tightly coupled electromechanical and turbomachinery systems needs to be coordinated and managed (Ref. 3). Due to the interdependence of subsystems, individual component faults and failures can severely impact the performance of the entire powertrain (Ref. 4). This paper presents and discusses an approach to monitor, detect, and mitigate such faults in the SUSAN powertrain, and demonstrates it in a piloted simulation.

The rest of this paper is organized as follows. In Section 2.0, the SUSAN powertrain is described. Section 3.0 introduces the definition of Integrated Vehicle Health Management and its relationship to fault recovery. Section 4.0 summarizes a thrust reallocation algorithm used to accommodate EE failures and saturations, while Section 5.0 presents it in the context of the SUSAN aircraft. This is followed by several examples demonstrating a powertrain fault recovery system in Section 6.0. Section 7.0 contains a discussion of the results, and Section 8.0 presents conclusions.

Figure 1.—Rendering of the current version of the SUSAN concept aircraft.

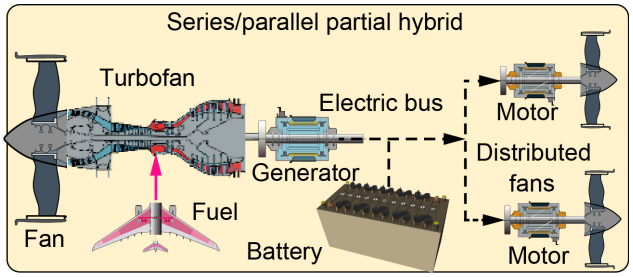

Figure 2.—Series/parallel partial hybrid EAP architecture.

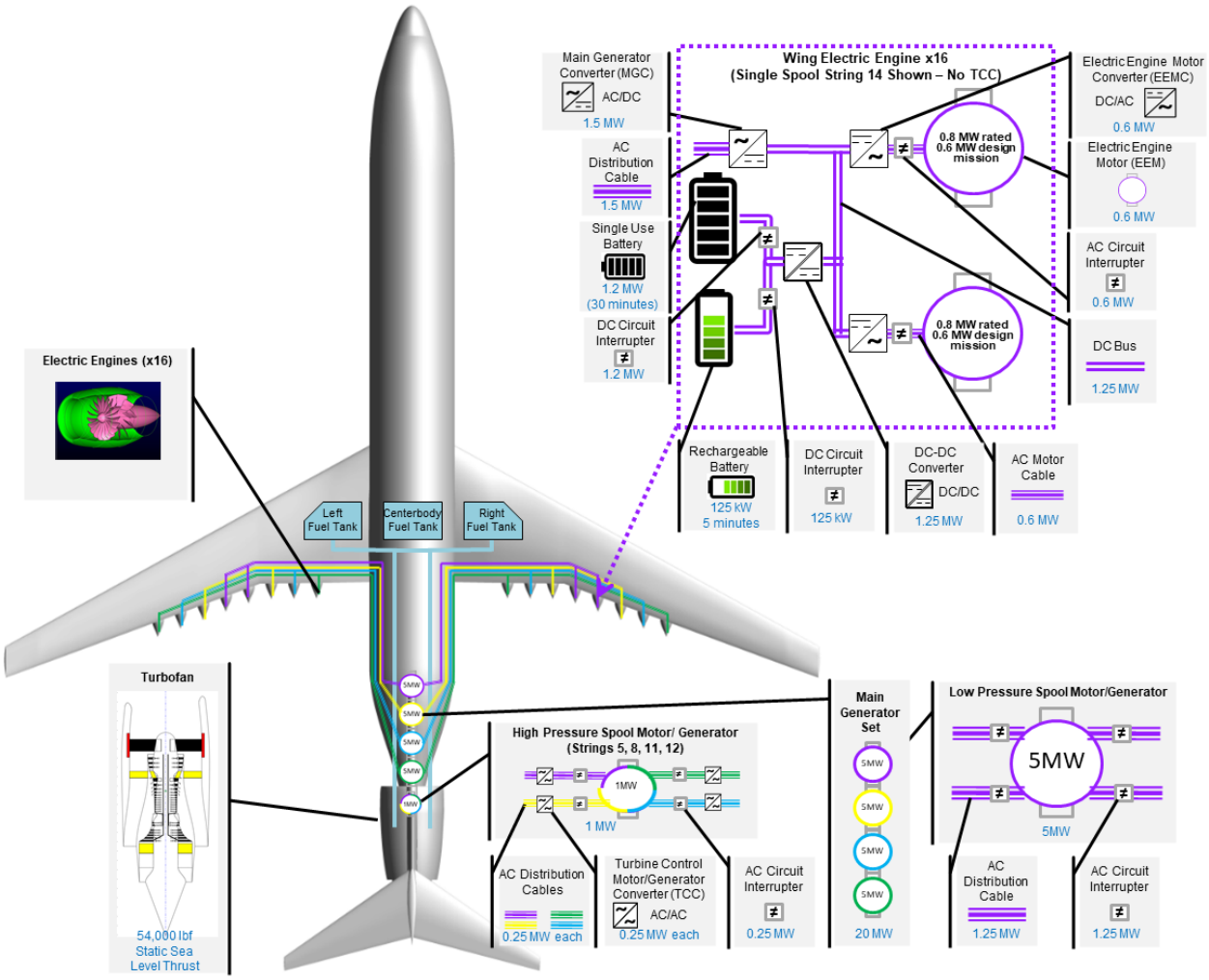

Figure 3.—Diagram of the SUSAN powertrain.

2.0 Powertrain Design

The fully integrated nature of the SUSAN vehicle makes the powertrain functionality central to the control design effort. As shown in Figure 3, the powertrain in its current configuration includes a single BLI GTE in the tail. Power is extracted from it through four 5 MW motor/generators (electric machines or EMs) connected to the Low Pressure Spool (LPS) and a single 1 MW EM on the High Pressure Spool (HPS). These generators are connected to AC buses that distribute power to operate the 16 EEs under the wings. The engines are numbered 1 to 17 from left to right from the pilot's point of view, with the centrally located GTE identified as number 9. Four three-phase power buses from each of the 5 MW main generators connect to four EEs symmetrically across the wings (1, 8, 10, 17), (2, 7, 11,16), (3, 6, 12,15), and (4, 5, 13, 14), as shown in Figure 4. This ensures that a generator failure will not result in thrust asymmetry. The 1 MW generator also has four three-phase power buses, one each attached to a single EE tied to each of the main generators (5, 8, 11, 12) (not shown in Figure 4). Although four buses share each generator, the power for each bus is demanded independently up to its 1.25 MW limit, based on component sizing. The components are designed such that throughout the flight envelope, the thrust is split 35% from the GTE and 65% from the EEs in total, which requires a large amount of power

extraction. Note that this implies that a thrust setting change will adjust the thrust of not only the GTE, but that of the EEs proportionally, too. Each of the 16 paths from a generator to an EE motor is called an electrical string, and each such string includes both AC and DC portions. A small rechargeable battery and a single-use emergency battery are both attached to each electrical string through a DC-DC converter (Figure 5). The rechargeable battery has multiple functions related to control and operation of the aircraft, including: providing a boost capability during climb, enabling rapid acceleration of the EEs, facilitating GTE operability improvements, and helping to maintain bus voltage.

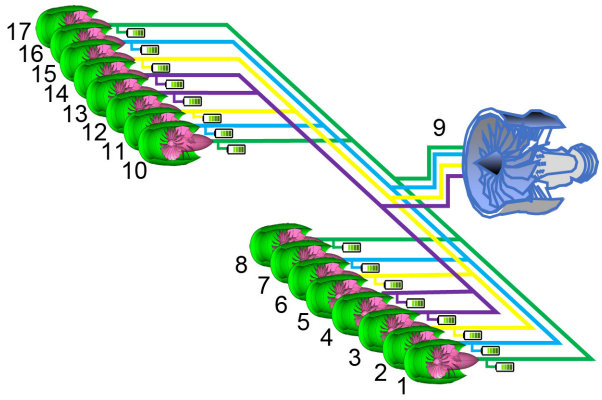

Figure 4.—SUSAN powertrain engine numbering.

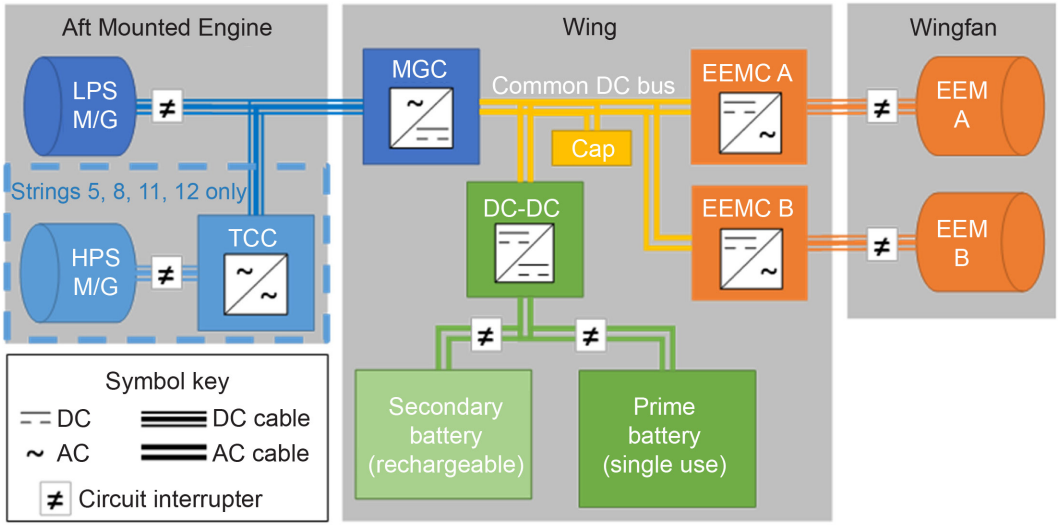

Figure 5.—SUSAN electrical power system string diagram. The acronyms are defined in Figure 3.

Unlike a traditional multi-engine aircraft in which pilots have individual throttle levers they can manipulate independently, the SUSAN powertrain operation is complex, and no pilot intervention is permitted beyond the movement of a single throttle (Ref. 5).[1] Furthermore, the Distributed Electric Propulsion (DEP) provides enhanced maneuverability that the flight control system can leverage. These interactions require the control system to coordinate multiple subsystems simultaneously, respecting the constraints of each. An advantage of this, indeed one that helps to optimize the overall vehicle, is that the design relies on the ability of the control system to facilitate the interactions. This coordination optimizes overall operation, which subsequently enables potential weight reduction benefits (Ref. 6).

3.0 Integrated Vehicle Health Management

An Integrated Vehicle Health Management (IVHM) system requires a multi-disciplinary approach that enables automatic detection, diagnosis, prognosis, and mitigation of adverse events arising from component failures (Ref. 7). SAE International calls this a Self-Adaptive Health Management System, which they define as self-adaptive control and optimization to extend vehicle operation and enhance safety in the presence of potential or actual failures (Ref. 8). This is the highest of SAE's six IVHM capability levels. The IVHM system supports redistribution of power to EEs in case of specific motor failures, and control reconfiguration in general. With SUSAN, it is anticipated that a vast array of potential powertrain faults will be handled automatically up to the limits of the system. The built-in redundancy allows EE failure and potentially even a generator failure to be accommodated without a significant performance impact. A GTE failure is mitigated using the primary batteries, although this situation necessitates an emergency landing (Ref. 9).

The DEP system of the SUSAN aircraft serves multiple critical roles in ensuring safe operation of the aircraft: it provides 65% of the thrust during normal operation and additional thrust during the boost phase of climb, it aids maneuvering as part of an integrated flight/propulsion control (IFPC) system, and it extracts an appropriate level of power to assure the performance and operability limits of the GTE. An IVHM system should maintain the functionality of the DEP system, even in the presence of multiple faults, fully utilizing the powertrain's intrinsic redundancy. Once the redundancy is exceeded, performance should degrade gracefully (Ref. 10).

4.0 Thrust Reallocation Algorithm

A thrust reallocation algorithm that accommodates EE failures and saturations, optimized to minimize power consumption, was derived and demonstrated in Reference 11. The approach addresses how the DEP commands are used to provide thrust and aide in maneuvering. The individual commands to the EEs from the IFPC system are adjusted, accounting for the efficiency of each electrical string to minimize the sum of the squares of power consumed by each EE, while maintaining the commanded forces and moments on the airframe. For brevity, the solution will only be summarized here.

The multiple EEs distributed along the wings are individually commanded to produce thrust. For each EE, the thrust multiplied by the distance from the centerline results in torque on the airframe. If the torques from both wings balance, there is no tendency for the plane to change heading; if there is an imbalance, the plane will turn toward the wing with the lower torque magnitude. Note that as long as total net thrust is correct, the thrust produced on one wing need not match that on the other. The problem

[1] Based on the current concept of nominal operation, but this is an area of on-going research.

formulation assumes a linear relationship between power and thrust, thus, individual EE power, p_i, as a function of net thrust, fn_i, is

$$p_i = a_1 fn_i + a_2 \tag{1}$$

the problem constraint is

$$Ax = b \tag{2}$$

where

$$A = \begin{bmatrix} 1 & \cdots & 1 \\ r_1 & \cdots & r_n \end{bmatrix} \tag{3}$$

where r_i is the distance from the ith EE to the centerline and

$$b = \begin{bmatrix} Fn \\ Q \end{bmatrix} \tag{4}$$

where Fn is the total net thrust produced by all EEs, and Q is the net torque on the aircraft due to differential thrust. η_i is the efficiency of the ith string, and

$$H=\text{diag}(\eta_1, \ldots, \eta_n) \tag{5}$$

The solution is

$$x = HA^T(AHA^T)^{-1}b + \frac{a_2}{a_1}(HA^T(AHA^T)^{-1} - I)[1 \cdots 1]^T \tag{6}$$

where x is the vector of thrust commands to the EEs (see Ref. 11). Furthermore, as explained in Reference 11, a variation of Equation (6) is used to redistribute the unable-to-be-met thrust command from each EE that is failed or saturated to the remaining available EEs in a continuous manner. This algorithm supports our definition of IVHM because it reconfigures and optimizes the control to extend vehicle operation and enhance safety in the presence of failures.

Figure 6 shows a scenario with EE thrust setpoint reallocation similar to one from Reference 11 where differential thrust was used to perform a coordinated turn, i.e., a turn in which there is no lateral acceleration. Here the electrical string efficiencies are not equal so the initial thrust values from the individual EEs are not equal. Additionally, once in the coordinated turn, the flight control uses the EE thrusts differentially to prevent sideslip. Three sequential EE failures are accommodated such that perfect setpoint tracking would result in perfect execution of the turn, i.e., perfect matching of total net thrust and torque on the aircraft resulting from the original flight control commands. Figure 7 shows the same scenario but not accounting for efficiencies, i.e., assuming they are equal, in which case there is no power savings achieved by redistributing the thrust. Here the thrust commands start off equal before spreading out for the turn. The thrust reallocation due to saturations (e.g., between about 58 and 62 s) is much more obvious here compared to Figure 6 because it is not obscured by the adjustment to account for string efficiency. Here again the total net thrust and torque on the aircraft exactly match that achieved by the baseline EE thrust commands from the flight control system.

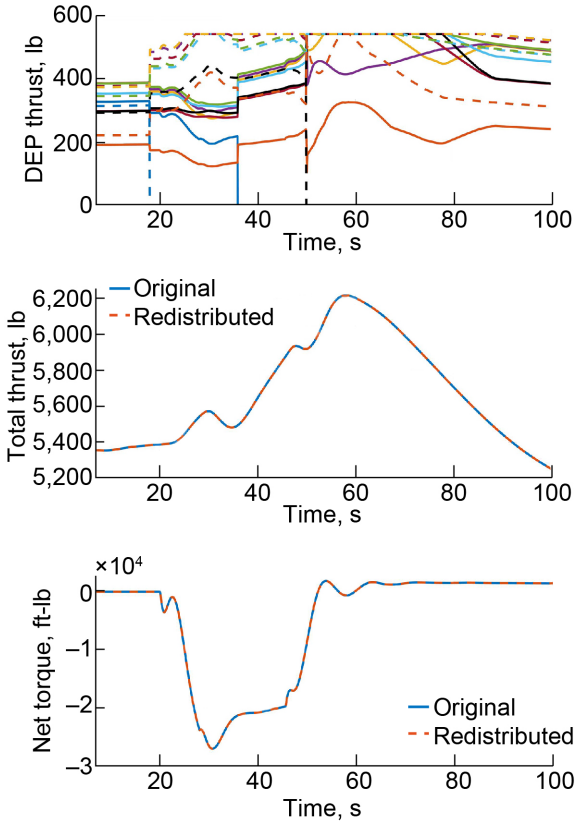

Figure 6.—Scenario with DEP used for turning. The string efficiencies are not equal. Here EEs 17, 1, and 10 fail sequentially, resulting in thrust reallocation to the remaining EEs. Several saturations occur throughout the turn, requiring a temporary reallocation of the unachievable thrust.

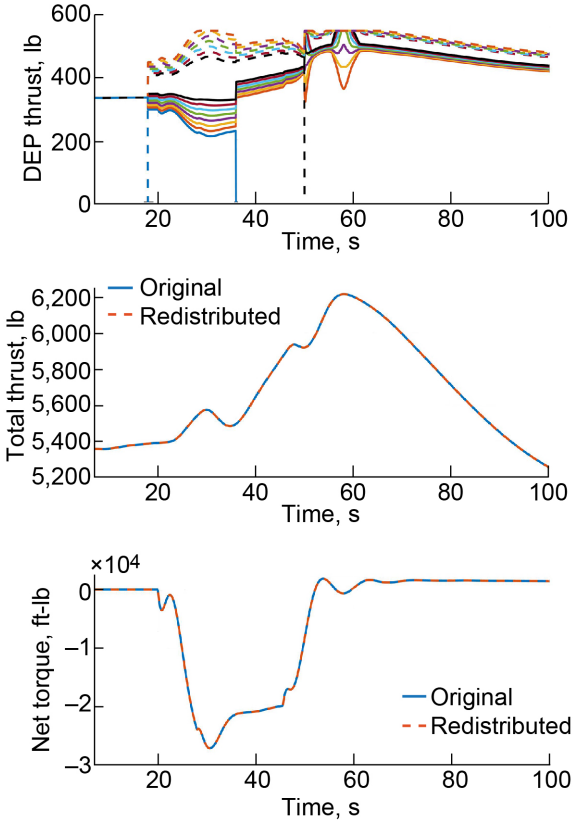

Figure 7.—Scenario with DEP used for turning. The string efficiencies are equal. Here EEs 17, 1, and 10 fail sequentially, resulting in thrust reallocation to the remaining EEs. Several saturations occur throughout the turn, requiring a temporary reallocation of the unachievable thrust.

5.0 System Development

If the algorithm described in the previous section is to be applied to the SUSAN aircraft, it must appropriately address the aircraft configuration and EE characteristics. Figure 8 is a front view of the aircraft showing the EE positioning from which distance from the centerline can be computed. Figure 9 shows the operating envelope of the power/propulsion system, and Figure 10 contains several EE characterization plots at multiple operating points within that envelope. Notably, the power vs. net thrust plot (lower left) indicates that they have a linear relationship throughout the envelope, as stated in Equation (1).

The portion of the IVHM system addressed by the thrust reallocation algorithm requires several pieces to be in place: the algorithm itself, an electrical string efficiency estimation scheme, and a fault detection system that identifies and annunciates faults in the electrical strings that will cause the associated EE to shut down. An efficiency estimation approach could use sensed current and voltage values to determine the power lost as heat through the electrical system and thus the ratio of EE power to extracted power, while accounting for bus capacitance and battery charging and discharging (Figure 5). For this work we can assume that the fault detection is incorporated in the electrical components themselves (Refs. 12 and 13).

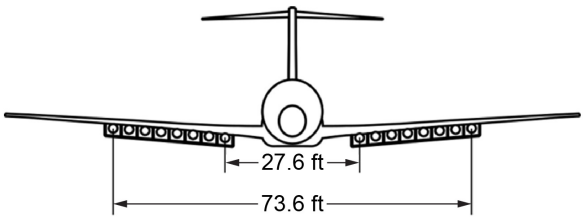

Figure 8.—SUSAN front view showing EE locations. The measurements indicate that the EEs are spaced about 3.3 ft on center.

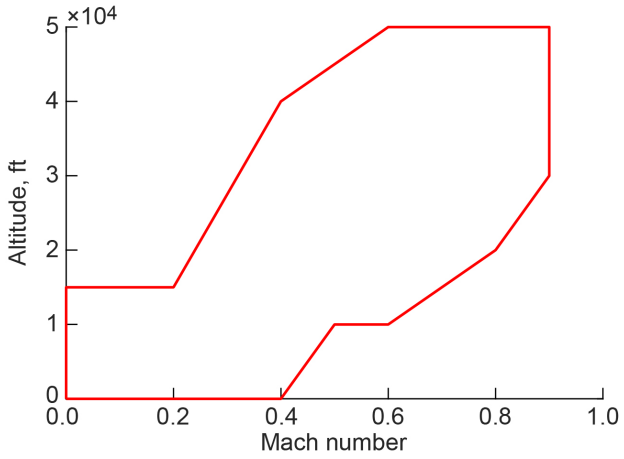

Figure 9.—SUSAN EE flight envelope. Standard day (dTamb = 0).

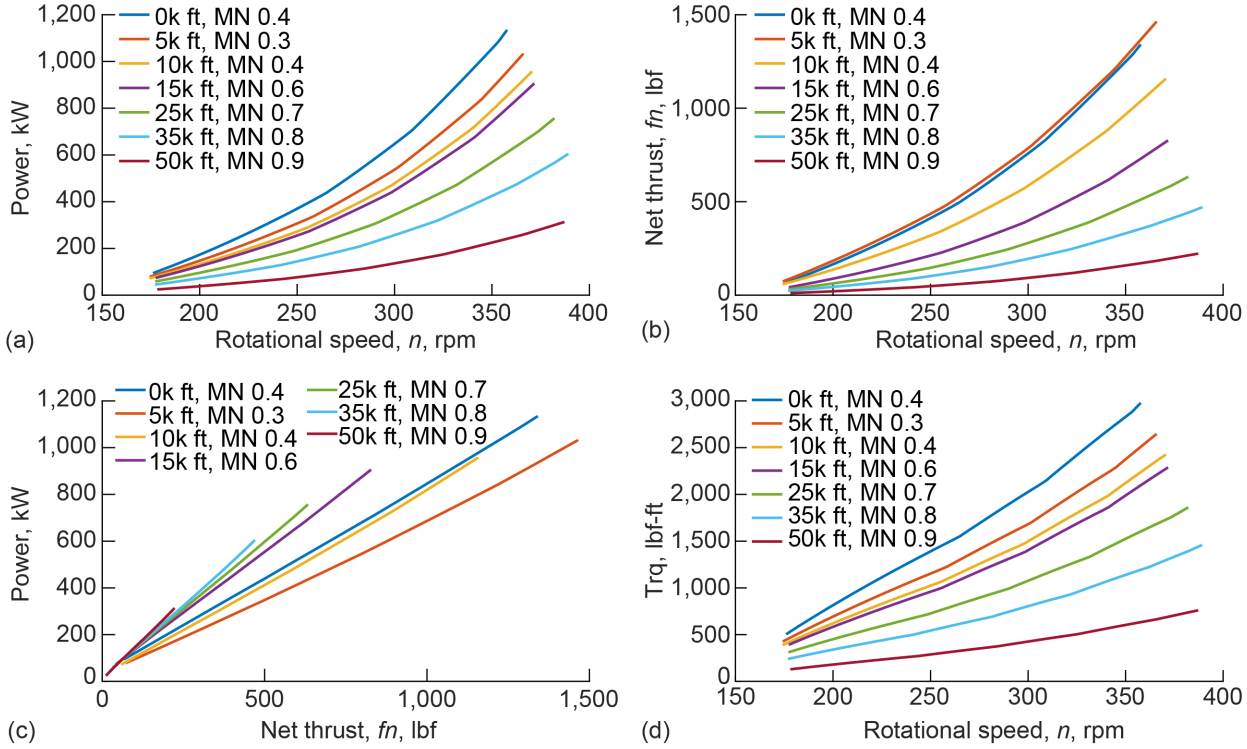

Figure 10.—Motor power, net thrust, and motor torque vs. fan rotational speed and motor power vs. net thrust at various flight conditions for a SUSAN EE. (a) EE motor power vs. shaft speed. (b) EE net thrust vs. shaft speed. (c) EE motor power vs. net thrust. (d) EE torque vs. shaft speed.

6.0 Powertrain Fault Recovery Examples

Before moving into the examples, it must be noted that a turn is initiated by rolling (Ref. 14), and whether the rudder or differential thrust is used for turn coordination, roll is impacted. This means that a certain amount of aileron is used to maintain the bank, but the amount required could vary, depending upon the location of the coordinating mechanism relative to the roll axis. The torque shown in Figure 6 and Figure 7 coordinates the turn in the yaw axis, but also influences roll. The flight simulator implementation will allow us to examine the effect thrust reallocation has on this axis of rotation.

The examples consist of a portion of a flight in a piloted flight simulator. For the sake of visual clarity and because of the lack of repeatability with a human pilot, the examples provide the simplest demonstration of the approach. Reference 11 compared a multiple failure scenario with a baseline coordinated turn with no faults to demonstrate that the thrust setpoint reallocation enabled theoretically perfect recovery assuming instantaneous fault identification; this also enabled an analysis of the power savings, which is related to fuel savings. In this paper, the piloted demonstration adds multiple complicating factors that justify a more straightforward approach: the pilot cannot exactly duplicate the scenario, making comparison to a fault-free case difficult and the lack of repeatability makes the power savings estimate unreliable. On the other hand, the simulation adds aircraft and EE dynamics, which gives a more realistic sense of how well the thrust reallocation works, it provides the opportunity for a multidimensional analysis of the results, and it enables real-time expert feedback of aircraft performance. In order to see how the system works without multiple confounding effects, two simplifications are made. First, the efficiency of all electrical strings is assumed to be the same, eliminating the need for an efficiency estimator and maintaining equal thrust commands to all EEs in fault-free flight. Second, the rudder is used for yaw control rather than DEP. Again, this maintains equal thrust commands to all EEs in fault-free flight. These two simplifications enable a very clear presentation of the results.

All examples begin with the aircraft trimmed at a cruise condition. Failures are sequentially injected, represented here by reducing the “failed” EEs’ thrust to idle. Then the pilot can evaluate the aircraft performance. The pilot’s evaluation covers handling qualities while the algorithm minimizes power extraction and performs thrust reallocation. Because the flight cannot be precisely duplicated, the power savings cannot be demonstrated, thus the identical efficiencies. The thrust reallocation can be demonstrated. It takes efficiency into account (Eq. (6)), so the fact that the efficiencies are the same does not change how the algorithm works, just the way the thrust is reallocated. Similarly, representing a failure by reducing an EE to idle only changes the amount of lost thrust to be made up, i.e., difference from flight idle vs. difference from windmilling drag, which is a value with a lot of uncertainty (Ref. 11). The pilot can fly and evaluate the performance of the aircraft before and after failures.

Three examples are presented next: 1. in which the pilot just observes the aircraft behavior as the failures occur; 2. in which the pilot moves the throttle as the failures occur but does nothing else to influence the aircraft behavior, and 3. in which the pilot attempts to maintain aircraft trim throughout the flight segment.

6.1 Example 1: Demonstration of Thrust Reallocation

Example 1 simply demonstrates the thrust reallocation in response to failures. Here the pilot trimmed the aircraft at a cruise condition before the sequential failures occurred; there is no autopilot to maintain attitude, so the aircraft reacts to changes in the propulsion system. Figure 11 shows the EE thrust commands based on throttle position (also called Power Lever Angle or PLA) as well as the actual resulting thrust values. The black dashed line indicates that the commands are the same for all EEs and remain so throughout this portion of the flight because the throttle position is maintained and there is no

differential thrust commanded. The other lines represent the dynamic thrust values of the individual EEs. They are initially the same, but as EEs drop to idle (representing a failure), the commands diverge according to Equation (6). At 60 s, EE 2 “fails,” followed by 1 at 90 s. The remaining EE thrusts spread out, increasing on average, to maintain both total thrust and net torque on the aircraft, but no EEs saturate. At 120 s, EE 17 “fails,” followed by EE 16 at 150 s. Without EE 17, the thrusts increase on average but move closer together as the sides are now more balanced. Once EE 16 drops to idle, the thrusts converge, but at a higher value than initially, since 12 EEs are now delivering most of the thrust originally provided by 16 EEs. As a check, the thrust of the four EEs at idle plus that of the 12 remaining EEs equals the sum of the original 16 thrust commands (black dashed line). Figure 12 shows the aircraft attitude changes during the portion of the flight that includes the EE failures. There are some minor undamped oscillations, indicative of an aircraft without stability augmentation. The main observation is that the aircraft starts to roll to the right once there are two EE failures on the left side. This is because, with the two outermost EEs on the left side failed, the total thrust produced by the remaining EEs on the left side exceeds that of those on the right to balance the torque on the aircraft. Furthermore, this left-side thrust is produced by the six inboard EEs, which are the lowest relative to the aircraft centerline (Figure 8), resulting in a pitch up moment on the left side. Once the two outermost EEs on the right fail, the thrust is again balanced and the roll no longer increases. Figure 13 shows the altitude, Mach, and heading over the same time period. Attitude and Mach each show a slight downward trend, which is probably due to the thrust setting being slightly too low, and the phugoid is evident. The heading change corresponds to the initiation of the roll and continues as the aircraft remains banked.

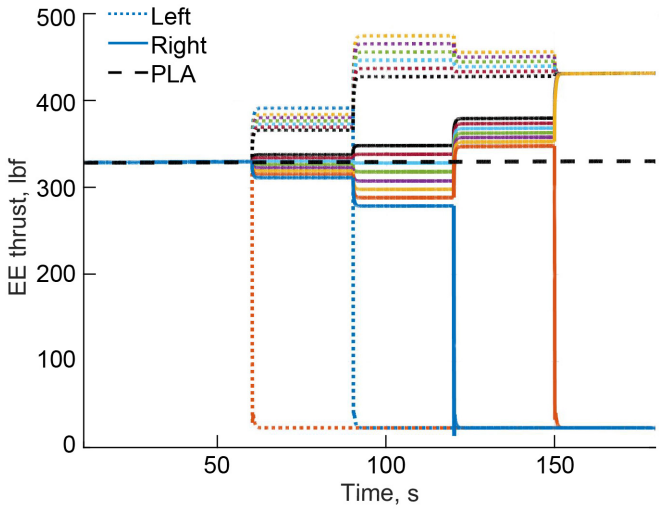

Figure 11.—Example 1: initial EE thrust commands based on the throttle setting (dashed line) and modified thrust values due to the reallocation algorithm both before and after failures. The throttle remains fixed throughout this portion of the flight. EE 2 fails at 60 s, EE 1 fails at 90 s, EE 17 fails at 120 s, and EE 16 fails at 150 s.

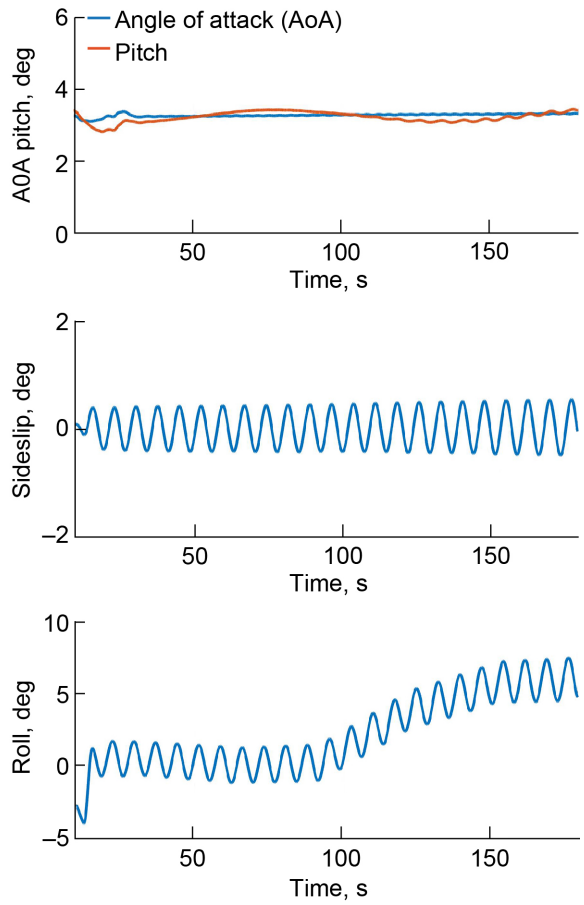

Figure 12.—Example 1: attitude changes in the example where the pilot did not touch the controls after trimming. Pitch has a long period phugoid as well as short period oscillations. Small synchronized undamped oscillations in sideslip and roll appear to be Dutch roll. Roll begins to increase at about 90 s and levels off at about 150 s, corresponding to the second and fourth EE failures.

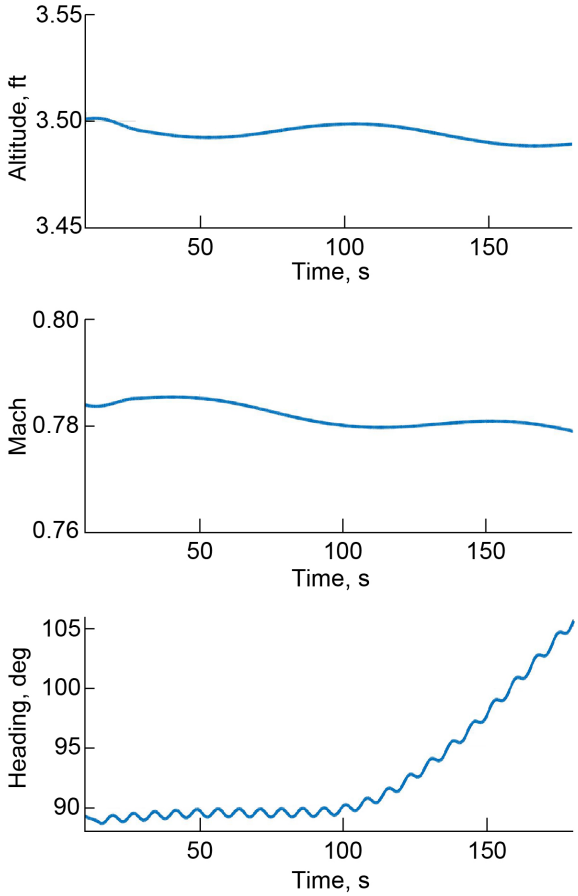

Figure 13.—Example 1: altitude, Mach, and heading changes in the example where the pilot did not touch the controls after trimming. There is a small downward trend in altitude and Mach, as well as a phugoid oscillation. The initiation of the heading change corresponds to the non-zero roll.

6.2 Example 2: Demonstration With Throttle Movements

In Example 2, again the pilot trimmed the aircraft before the failures began, but then actively moved the throttle during the sequence of failures. The black dashed line in Figure 14 indicates the commands for all EEs based on throttle position. Again, there is no active autopilot to maintain attitude, so the aircraft reacts to changes in the propulsion system. As in the previous example, there are a sequence of failures (EE 16 at 20 s, 17 at 30 s, 1 at 60 s, 2 at 70 s), but here the pilot began moving the throttle immediately after the first failure. Although the thrusts separated, no EEs saturated after the first failure. With the increased throttle, however, the second failure caused the remaining EEs on the right side to saturate. The further throttle increase caused additional saturations, and the subsequent throttle decrease enabled some of the EEs to unsaturate. With the third failure, all saturated EEs unsaturated, and with the fourth failure the thrusts reconverged. Figure 15 shows the aircraft attitude changes during the portion of the flight that includes the EE failures and throttle movement. The top plot shows pitch and angle of attack, which are essentially the same, indicating level flight, until the increase in throttle setting just after

20 s (black dashed line in Figure 14). At this point, the pitch increased as the aircraft started to climb until the pitch leveled off and then decreased with the throttle reduction beginning at about 50 s; the aircraft subsequently began to descend (Figure 16 top). Angle of attack remained essentially constant throughout the altitude changes. The middle plot in Figure 15 shows sideslip, which remained at about zero until the second EE failure at 30 s, at which point it initiated a small oscillation (recall there is no autopilot to damp oscillations). The third plot displays roll, which also stayed near zero until the second EE failure. At this point, the roll increased at a fairly consistent rate until the third EE failure at about 60 s, when the roll rate (ignoring oscillations) returned to zero. This left the aircraft rolled at just below 5°, albeit with consistent small oscillations, which could be easily damped by an autopilot. Figure 16 shows small deviations in altitude and Mach that match up with changes in pitch. These could be due to throttle movements, EE failure, or indicate a possible phugoid, although the portion of the flight is too short to observe the whole period. As in the previous example, there is a heading change, which corresponds to non-zero roll.

Closer examination of this example reveals an interesting phenomenon. As in the first example, the aircraft rolled to the right after the second EE failure, but unlike the first example, here the failures occurred on the right side first. This can be explained by looking at Figure 17, which shows commanded and achieved total thrust and net torque on the aircraft. Between the second and third EE failures (from 30 to 60 s) commanded thrust and torque could not be achieved simultaneously, causing an imbalance that rolled the aircraft to the right. Still, the attitude changes are small and could be handled easily by an autopilot.

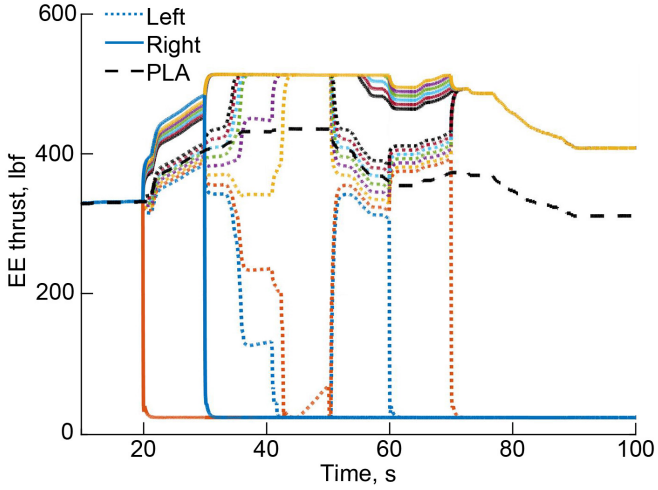

Figure 14.—Example 2: initial EE thrust commands based on PLA (dashed line) and modified thrust values due to the reallocation algorithm both before and after failures. The throttle is moved during this portion of the flight. EE 16 fails at 20 s, EE 17 fails at 30 s, EE 1 fails at 60 s, and EE 2 fails at 70 s.

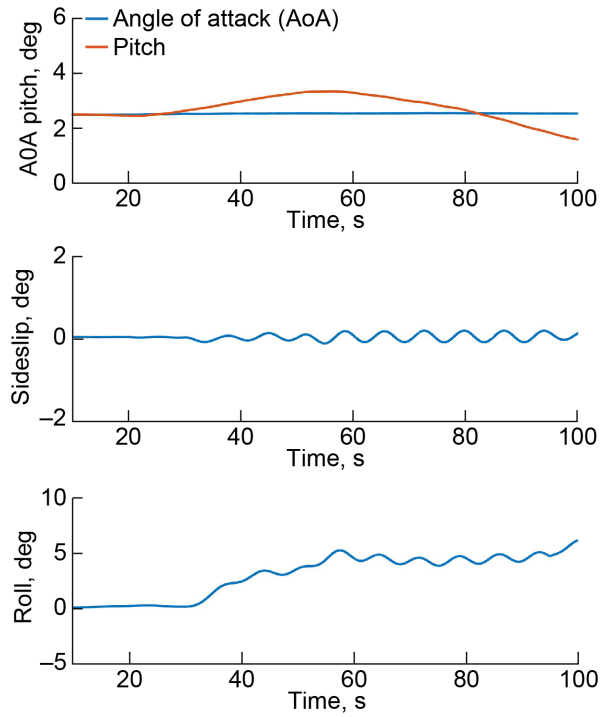

Figure 15.—Example 2: attitude changes in the example where the pilot moved the throttle lever. Pitch varies as the aircraft climbs then descends, while small undamped oscillations develop in both sideslip and roll, presumably Dutch roll. The roll offset occurs while there is a temporary asymmetry of the failures.

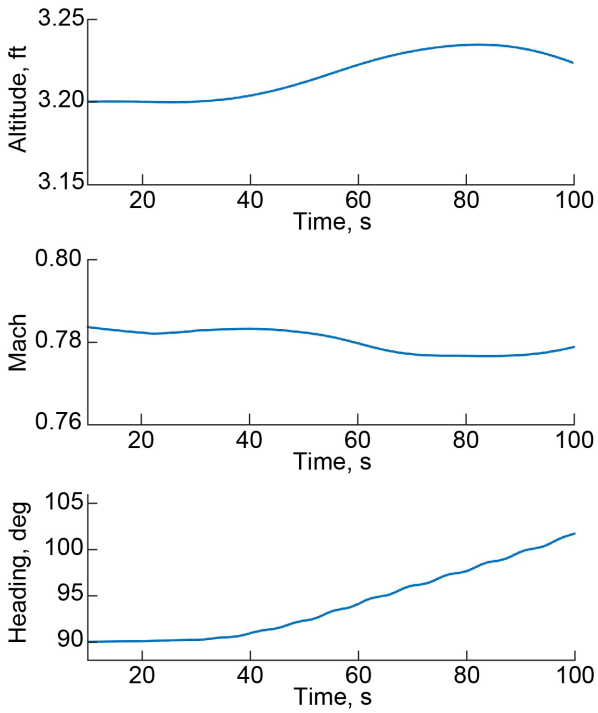

Figure 16.—Example 2: altitude, Mach and heading changes in the example where the pilot moved the throttle lever. There is a small increase in altitude of under 400 ft, while Mach number is initially dropping, then levels out and begins to drop again, then levels off. The initiation of these changes, along with that of pitch, appears to correspond to the timing of the second EE failure. The change in heading corresponds to the non-zero roll.

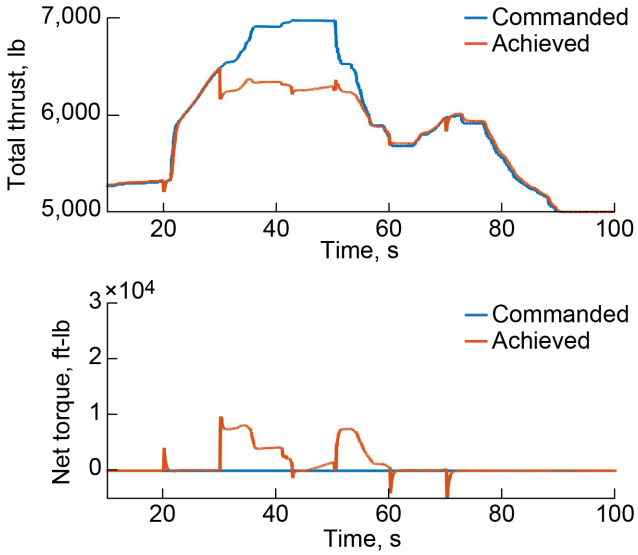

Figure 17.—Example 2: commanded thrust and torque based on PLA and achieved despite failures and saturations. The spikes visible at 20, 30, 60, and 70 s correspond to the dynamics of the failures and subsequent recovery.

6.3 Example 3: Demonstration With the Pilot Actively Trying to Maintain Straight and Level Flight

In Example 3, the pilot hand flew the aircraft, attempting to keep it trimmed at cruise. The pilot made small aileron and elevator trim adjustments throughout the flight, using the instrument displays (Figure 18) and horizon for guidance. The pilot did not move the throttle since the thrust setting appeared to be correct for the cruise condition, nor did the pilot adjust the rudder. Figure 19 shows the thrust command based on the throttle position (black dashed line) and the dynamic EE thrust values, which separate and come back together with successive EE failures, tracking the thrust command on average when accounting for the "failed" EEs at idle. Figure 20 shows the aircraft attitude throughout the portion of the flight. The deviations are small and appear to be more related to pilot inputs than to the EE failures. Figure 21 shows changes in altitude, Mach number, and heading. These, too, are small, with heading changes resulting from roll. Pilot activity is shown in Figure 22.

Figure 18.—Annotated pilot display showing relevant aircraft variables. The EE thrust bars in the upper right indicate that EEs 1, 2, 16, and 17 have failed.

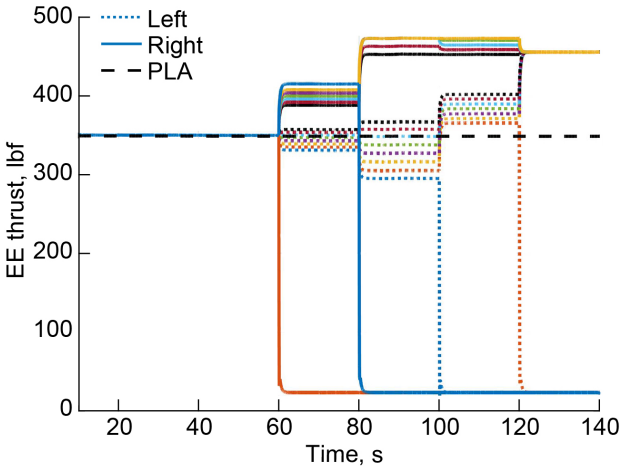

Figure 19.—Example 3: where initial EE thrust commands based on throttle setting (dashed line) and modified thrust values due to the reallocation algorithm both before and after failures. The throttle remains fixed throughout this portion of the flight. EE 16 fails at 60 s, EE 17 fails at 80 s, EE 1 fails at 100 s, and EE 2 fails at 120 s.

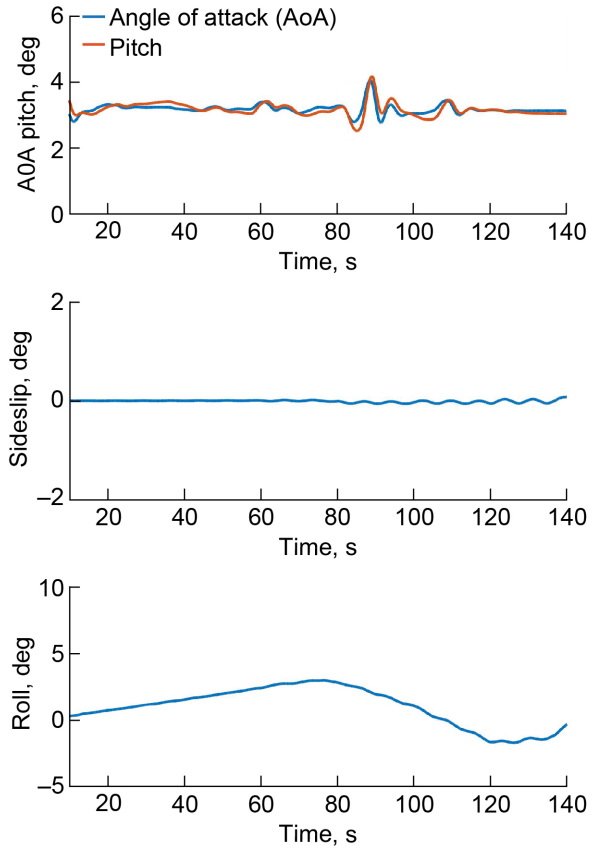

Figure 20.—Example 3: aircraft attitude as pilot attempted to maintain trim. A small Dutch roll is evident, apparently initiated by the first EE failure. Pitch and angle of attack align very well. Roll is initially increasing until adjustments are made.

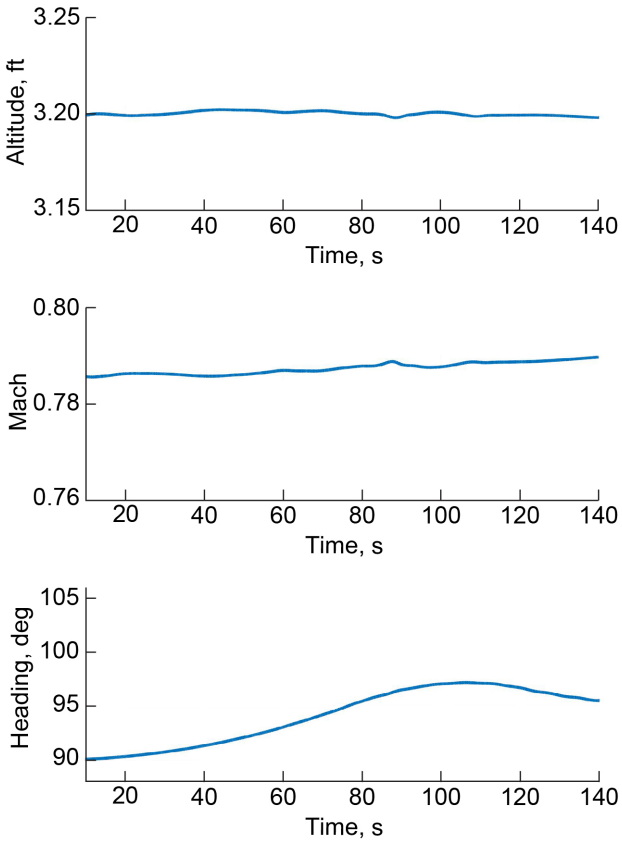

Figure 21.—Example 3: altitude, Mach, and heading as pilot attempted to maintain trim. There are slight altitude and Mach variations. Heading changes seem related to roll. None of these variations appears to be due to failure recovery.

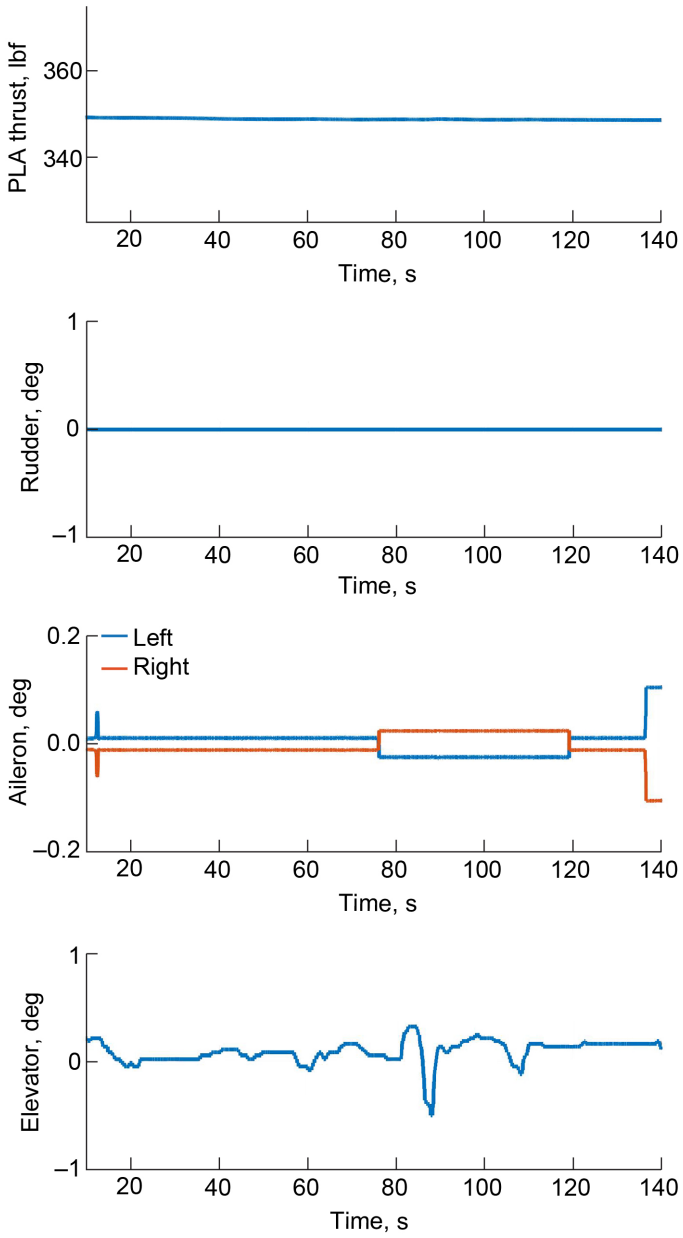

Figure 22.—Example 3: pilot's control surface deflections to maintain aircraft trim.

7.0 Discussion

The examples demonstrated good recovery of thrust and torque on the aircraft in response to EE failures, with only minor disturbances in aircraft attitude. The pilot commented that in normal flight, these types of disturbances would be hardly noticeable and easily compensated. The pilot specifically mentioned that EE failures on one side seemed to cause a slight roll in the opposite direction, as was noted in Example 1.

To be clear, the purpose of the thrust reallocation portion of the IVHM system is to maintain total thrust and net torque to the extent possible, and then gracefully degrade. This means that once redundancy is exhausted, it should still balance the constraints in a way that safely approximates a fully functional

system. It does not have to maintain aircraft attitude, as that is handled by the autopilot. Example 2, in which the pilot moved the throttle causing saturations, was particularly remarkable because for a short time all EEs were saturated (Figure 14), yet the aircraft response was not unexpected.[2] Closer examination shows that even when some of the EEs were unsaturated, there was still not sufficient redundancy to satisfy both constraints (Figure 17). This is an example of when the limits of the powertrain are exceeded, yet the system performed gracefully during that time. That is, although the total thrust and net torque on the aircraft could not track their commanded values (based on PLA), aircraft performance was resilient to the deviations, experiencing only a minor disturbance. The aircraft remained in a 5° roll once the symmetrical failures occurred, bringing thrust and torque back into balance. It would require a roll command or imbalance in the opposite direction to bring the wings back to level. In Examples 1 and 2, the pilot purposely did not make trim adjustments. Thus, while the examples demonstrate the aircraft's response to the thrust reallocation, it is not representative of how an aircraft would behave if the failure scenario occurred in an actual flight.

In Example 3, the pilot attempted to maintain trim without an autopilot. Here the pilot did a particularly noteworthy job in minimizing deviations. In general, it seems that the pilot's adjustments were in response to normal deviations due to imperfect trim and not related to failures. The small Dutch roll could have been initiated by a disturbance caused by a failure and recovery.

Only three examples are shown here, but the pilot performed many more tests. In the cases where the pilot initially trimmed the aircraft and then just observed, the results were very sensitive to the initial condition, i.e., how close to perfectly trimmed the aircraft was before the EE failures. If trimmed well, the aircraft showed little deviation for the duration of the short flight segment, even with the failure-induced disturbances. However, when not trimmed quite as well, the aircraft would deviate more quickly, possibly approaching a spiral mode. The pilot's observation was that the effects of the failures and ensuing thrust reallocation were very gentle. The quality of the initial trim attempt seemed to have a much more significant impact on the subsequent aircraft behavior. The takeaway is that during normal hand flying, the aircraft response to the failure recovery would be almost imperceptible and the pilot's continued engagement would keep the aircraft on course. It is likely that under autopilot control, the thrust reallocation would only be evident by looking at the displays. Even in the cases where saturations occurred, the pilot reported little performance decrease. It must be noted here that the pilot was aware of the EE failures and saturations, so was careful to avoid aggressive inputs.

These examples demonstrated that with proper thrust reallocation for the specific set of failures, performance is essentially maintained, and therefore, controllability and maneuverability are not compromised, even with multiple EEs inoperative. This is related to certain current FAA airworthiness standards for transport category airplanes (e.g., 14 CFR § 25.143-149). Certification considers both the likelihood of a hazardous event and the severity of its effects. Reference 4 discusses certification of aircraft with electrified powertrains in the context of current FAA standards, specifically addressing the tightly coupled, interacting subsystems. For the SUSAN powertrain, EE failures pose a risk mainly because of loss of thrust, but maneuverability and power extraction, which affects GTE operability, may also be affected. While the SUSAN powertrain was designed with a lot of redundancy, there is also the opportunity for multiple EE failures to occur, for example, loss of a generator or encountering a flock of birds with resulting bird strikes. Use of an IVHM system that takes advantage of the redundancy to reallocate lost thrust can mitigate the effect of the failures. Systematic testing and analysis with various numbers and combinations of EE failures will determine the limits of the algorithm to fully recover lost

[2] The aircraft rolled toward the failed EEs in Example 2, which was the opposite of what happened in Example 1. In traditional multi-engine aircraft without DEP and thrust reallocation, an engine failure will result in a roll towards the failed engine, so generally speaking, a pilot will expect to see roll accompanying an engine failure.

thrust and torque; successful cases will have a negligible safety effect. Further evaluation will determine the severity of events for which thrust and torque cannot be fully recovered, but reduced capability does not necessarily imply reduced safety. As powertrain performance gracefully degrades, it may place restrictions that result in modifications on the operation of the vehicle to maintain safety.

8.0 Conclusion

The examples of recovery from in-flight electric engine failures in the SUSAN concept aircraft demonstrated that the thrust reallocation algorithm works as designed. The resulting minor attitude changes could be easily compensated with an autopilot. A more complete test that incorporates electrical string efficiency variation and an efficiency estimator, demonstrated over a range of flight conditions would provide additional confidence that such a health management approach could be successfully implemented. However, it was shown that the linear relationship between thrust and power assumed in the derivation of the optimal solution holds throughout the flight envelope, meaning that the algorithm should be successful everywhere. The automatic thrust reallocation in response to identified faults is well-suited to the control approach taken with the SUSAN concept. The complexity of the SUSAN powertrain and the interdependence of the parts means that the pilot will have limited control over individual subsystems, so a powertrain control that automatically takes advantage of the inherent redundancy to be robust to failures is critical to the safe operation of the vehicle.

References

1. Jansen, R.H., et al., "Subsonic Single Aft Engine (SUSAN) Transport Aircraft Concept and Trade Space Exploration," AIAA 2022-2179, *AIAA SciTech Forum*, San Diego, CA, and virtual, 3-7 January 2022.
2. Haglage, J.M., Dever, T.P., Jansen, R.H., and Lewis, M.A., "Electrical System Trade Study for SUSAN Electrofan Concept Vehicle," AIAA 2022-2183, *AIAA SciTech Forum*, San Diego, CA & virtual, 3-7 January 2022.
3. Sachs-Wetstone, J.J, Litt, J.S., Kratz, J.L., Buescher, H.E., "SUbsonic Single Aft eNgine (SUSAN) Power/Propulsion System Control Architecture Updates," AIAA-2024-1330, AIAA SciTech 2024 Forum, Orlando, FL, January 8-12, 2024.
4. Litt, J.S., Sachs-Wetstone, J.J., Simon, D.L., Sowers, T. S., Owen, A. K., Bell, M.E., Guthrie, B.E., Lehan, J., and Castro, A., "Flight Simulator Demonstration of Powertrain Failure Mitigation in a Partial Turboelectric Aircraft," AIAA 2023-4156, AIAA Aviation 2023 Forum, 12-16 June 2023, San Diego, CA and Online.
5. Arthur, J.J, Hill, M., Etherington, T.J., Sachs-Wetstone, J.J., Litt, J.S., Owen, A.K., "Flight Deck Display of Hybrid-Electric Propulsion State for the Subsonic Single Aft Engine (SUSAN) Transport Aircraft," AIAA-2024-1522, AIAA SciTech 2024 Forum, Orlando, FL, January 8-12, 2024.
6. Litt, J.S., Kratz, J.L., et al., "Control Architecture for a Concept Aircraft with a Series/Parallel Partial Hybrid Powertrain and Distributed Electric Propulsion," AIAA 2023-1750, SciTech Forum, 23-27 January 2023, National Harbor, MD.
7. Divakaran, V.N., Subrahmanya, R.M., and Ravikumar, G.V.V, Integrated Vehicle Health Management of a Transport Aircraft Landing System, white paper, https://www.infosys.com/engineering-services/white-papers/documents/aircraft-landing-gear-system.pdf
8. SAE International, Integrated Vehicle Health Management, Rev. 2, April 2018.

9. Denham, C.L., and Jansen, R.H., “Initial Regulatory and Certification Approach for the SUSAN Electrofan Concept,” AIAA 2022-2180, AIAA SciTech 2022 Forum, San Diego, CA & Virtual, Jan 2022.
10. Edwards T.E., and Lee, P.U. “Designing Graceful Degradation into Complex Systems: The Interaction Between Causes of Degradation and the Association with Degradation Prevention and Recovery,” AIAA 2018-3510, Aviation Technology, Integration, and Operations Conference, 25-29 June 2018, Atlanta, GA.
11. Litt, J.S., “Optimal Control Allocation for Distributed Electric Propulsion in a Series/Parallel Partial Hybrid Powertrain,” NASA/TM-20240008991, September 2024.
12. Lu, L., Han, X., Li, J., Hua, J., and Ouyang, M., 2013, “A Review on the Key Issues for Lithium-Ion Battery Management in Electric Vehicles,” Journal of Power Sources, 226, pp. 272–288.
13. Buescher, H.E., Culley, D.E., Bianco, S.J., and Connolly, J.W., et al., “Hybrid-Electric AeroPropulsion Controls Laboratory: Overview and Capability,” AIAA 2023-0671, 2023.
14. Langewiesche, W., *Stick and Rudder: An Explanation of the Art of Flying*, McGraw-Hill, New York, Chap. 12.